Anal. Bioanal. Electrochem., Vol. 16, No. 6, 2024, 568-594
https://www.doi.org/10.22034/abec.2024.714088

Analytical & Bioanalytical Electrochemistry

Full Paper

Investigating Quinazolinone Derivatives as Corrosion Inhibitors for Mild Steel in 1.0 M HCl: Experimental Insights, DFT Calculations, and MC Simulations

Hind Malki,[1] A.A. EL Hassani,[2] Sara El Hamzi,[3] Nadia Dkhirech,[1] Issam Forsal,[4,*] Fatima Elhajri,[5] Zakaria Benzekri,[5,6] A.T. Benjelloun,[2] and Said Boukhris[6]

[1]*Advanced Materials and Process Engineering, Faculty of Sciences, Ibn Tofaïl University, PO Box 133, 14000, Kenitra, Morocco*
[2]*Laboratoire d'Ingénierie, Modélisation et Analyse des Systèmes, LIMAS, Faculté des Sciences Dhar El Mahraz, Université Sidi Mohammed Ben Abdellah, USMBA, BP 1796, 30000 Atlas, Fès, Morocco*
[3]*Physical chemistry of processes and materials laboratory, Faculty of Science and Technology, Hassan I Settat University, Morocco*
[4]*Laboratory of Engineering and Applied Technologies (LITA), Department of Process Engineering, Sultan Moulay Slimane University, Shcool of Technology, Beni Mellal, Morocco*
[5]*Laboratory of Organic Chemistry, Catalysis and Environment, Department of Chemistry, Faculty of Sciences, Ibn Tofail University PO Box 133, 14000, Kenitra, Morocco*
[6]*Laboratory of Heterocyclic Organic Chemistry, Mohammed V University in Rabat, Faculty of Sciences Av. Ibn Battouta, BP 1014 Rabat, Morocco*

*Corresponding Author, Tel.: +212661118208
E-Mail: forsalissam@yahoo.fr

Received: 23 February 2024 / Received in revised form: 23 June 2024 / Accepted: 26 June 2024 / Published online: 30 June 2024

Abstract- This work reports on an inhibition and adsorption performance study of two quinazoline derivatives ((2-(2-chlorophenyl)-2,3-dihydroquinazolin-4(1H)-one) and (2-(2,4-dichlorophenyl)-2,3-dihydroquinazolin-4(1H)-one)) named ZB3 and ZB4, which were synthesized and examined using carbon nuclear magnetic resonance (^{13}C NMR) and proton nuclear magnetic resonance (^{1}H NMR) spectroscopy. The assessment of the corrosion prevention of these two compounds for MS in 1.0 M HCl was performed employing potentio-dynamic polarization (PDP) and (EIS) electronic impedance spectroscopy. The experiments performed showed that both derivatives operate well to prevent corrosion and their efficiencies exceed 85% at a concentration of 10^{-3}. Moreover, it is discovered that the three chemicals' adsorption on the m-steel surface complies with Langmuir adsorption isotherm equation. The

m-steel surface submerged in the corrosive solution was characterized by scanning electron spectroscopy (SEM) in conjunction with energy dispersive spectroscopy (EDS), spectroscopy using atomic force microscopy (AFM), X-Ray diffraction, and FTIR analysis. The findings showed that the examined inhibitors are well adsorbed, generating a barrier layer for the m-steel's surface. DFT calculations and Monte Carlo (MC) simulation were used to directly correlate the electronic and adsorption properties, respectively, with the experimental corrosion inhibition efficiencies obtained for quinazoline and its 2 investigated derivatives.

Keywords- Corrosion inhibition; Quinazolin derivatives; SEM/EDX; FT-IR; XRD; ICP-OES; DFT calculations; MC simulations

1. INTRODUCTION

In general, corrosion is described as the degradation of metallic materials, namely mild steel and their alloys due to their excellent mechanical properties, through reactions with environmental constituents [1]. Considering the very high socio-economic and irreparable harm due to corrosion, various corrosion mitigation methods, especially for pickling processes and industrial cleaning that use very aggressive solutions such as chloridric acid (HCl), have been developed [2]. Due to their strong ability to suppress corrosion and simplicity in synthesis and application, using organic compounds is one of the recognized ways that is most efficient, well-liked, and economical [3,4]. The creation of a protective coating that separates the metals from hostile surroundings is caused by the adsorption of these chemicals on the metal surface [5], which induces to the decrease of the corrosion rate. This adsorption is primarily due to a number of physicochemical properties of the molecule, including the group's function, electron density of the donor atoms, and potential steric impacts [6], which is the substitution effect on the inhibition potential [7].

Over the years, various organic substances have reportedly been shown to be excellent corrosion inhibitors. Two imidazole compounds with inhibitory efficiency of up to 96% for mild-steel in 1.0 M HCl were recently published by Ouakki et al [8]. In an additional study, Rbaa et al determined an inhibition efficiency of over 90% for two quinoline derivatives in 1.0M HCl for mild steel [9]. With an effectiveness of nearly 98%, Tazouti et al. assessed three quinoxaline derivatives for their ability to prevent mild steel corrosion in acidic conditions [10]. Errahmany et al studied new quinazoline derivatives (1.0 mol L^{-1}) and obtained between 80% and 95% anticorrosion efficiency for mild steel in 1M HCl medium [11].

The study on investigating Quinazolinone derivatives as corrosion inhibitors for mild steel in 1.0 M HCl revealed significant findings regarding the inhibition and adsorption performance of the quinazoline derivatives. The results indicated rapid inhibition of steel dissolution in the presence of the inhibitors studied. DFT calculations and MC simulations were conducted to understand the corrosion inhibition mechanism of the quinazolinone derivatives. The structural analysis showed the effect of substituting hydrogen atoms with chlorine atoms on the inhibitory efficiencies of the derivatives. Molecular electrostatic potential (MEP) simulations were used

to predict the reactive regions of the molecules under electrophilic and nucleophilic attacks, providing insights into the inhibitory action of the compounds.

The implications of this research are significant for the development of effective corrosion inhibitors for mild steel in acidic environments. By studying the molecular structures of the derivatives and their abilities to inhibit corrosion through Monte Carlo simulations and DFT calculations, a deeper understanding of the inhibitory properties of the compounds was achieved. This research contributes to the ongoing efforts to design and optimize organic substances as corrosion inhibitors, with the potential to enhance the protection of mild steel in corrosive environments.

Overall, the combination of experimental insights, theoretical calculations, and surface analysis techniques employed in this study offers valuable insights into the development of corrosion inhibitors and their application in protecting mild steel from corrosion in acidic conditions.

This study's goal is to evaluate the anticorrosive property of two quinazolinone derivatives: (2-(4-chlorophenyl)-2,3-dihydroquinazolin-4(1H)-one) and (2-(2,4-dichlorophenyl)-2,3-dihidroquinazolin-4(1H)-one) on mild steel in an acidic environment (HCl 1 mol L^{-1}). These two chemicals are being synthesized and characterized employing ^{1}H and ^{13}C NMR spectroscopy, a method described by Z.Benzekri et al [12]. Electrochemical measurements have been carried out to determine the inhibitory action of the two organic compounds. Surface analysis of mild-steel was performed via SEM/EDS, X-Ray diffraction, FT-IR, and AFM spectroscopy. To establish a correlation between the molecular structures of the examined derivatives and their abilities to inhibit corrosion, Monte Carlo (MC) simulations and DFT calculations were also performed.

2. EXPERIMENTAL SECTION

2.1. Materials and Solutions

The mild steel used in this study to conduct all of the corrosion experiments was made up of the following elements (in weight percent): 0.09% P, 0.38% Si, 0.01% Al, 0.05% Mn, 0.21% C, 0.05% S and the rest Fe. The MS samples were polished with abrasive paper at different grain, cleaned with distilled water, degreased with acetone, and then allowed to air dry. The two quinazolinone derivatives were prepared with concentrations ranging from 10^{-6} M to 10^{-3} M, and a blank solution was generated for comparison. While obtaining the aggressive HCl solution (1.0 mol/l) required a dilution of concentrated HCl (37%) with filtered water.

2.2. Synthesis of organic compounds (ZB3 & ZB4)

Aromatic aldehyde (4-Chlorobenzaldedehyde (**1a**), 2,4-Dichlorobenzaldedehyde (**1b**)) (1 mmol), 2-aminobenzamide 2 (1 mmol), & $(N_2H_5)_2SiF_6$ [13] (0,1 mol%) in 2 ml of ethanol,

were heated to 80 °C by stirring. TLC (eluent: ethyl acetate: oil ether (1: 4, v/v)) follows the usual. Hot ethanol is added to the reaction mixture once the reaction is finished. The $(N_2H_5)_2SiF_6$ has been recovered by basic filtration. After cooling, ethanol was used to re-crystallize the filter (Figure 1).

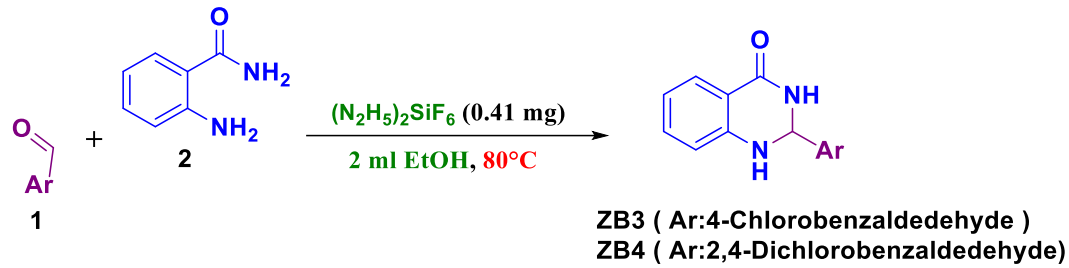

Figure 1. Synthesis of 2,3-dihydroquinazolin-4(1H)-ones ZB3-ZB4

2.3. Electrochemical measurements

Electrochemical experiments had been performed under a temp of 298K by employing a three-electrode cell equipped with a Gamry-potentiostat interface 1010E. A mild steel working electrode (with 1.0 cm^2 of surface area that is exposed.), an ultrapure platinum foil counter electrode, in addition to an Ag/AgCl reference electrode. The mild-steel then extended in a 1M chloride acid solution for thirty minutes till the steady-state open circuit potential (OCP) was achieved using a frequency range between 100 kHz to 0.1 Hz.

The following is how the anticorrosive performance is calculated using the corrosion current density data [14]:

$$\eta pp = [(i^0_{corr} - i_{corr}) / i^0_{corr}] \times 100 \quad (1)$$

$i°_{corr}$ and i_{corr} indicate the corrosion current density before and after the addition of chemical inhibitors (ZB3 and ZB4).

$$\eta_{EIS} = [(R_{ct} - R^0_{ct}) / R_{ct} \times 100] \quad (2)$$

$R°_{ct}$ and R_{ct} correspond to the polarization resistance without as well as with the inclusion of inhibitors (ZB3 and ZB4).

2.4. Surface analysis

2.4.1. Scanning Electron Microscopy (SEM/EDS)

The morphology of the films deposited on the M-S surface 6 hours after immersing in 1.0 M HCl before and with the addition of both inhibitors (ZB3 and ZB4) was examined by an EDX analysis and a Quantra 450 scanning electron microscope.

2.4.2. X-Ray Analysis

After immersing the steel samples' surface in both the free and inhibited solution for 6 hours, XRD examination was carried out. The model XRD X' PERT PRO MD was employed to assess the surface of the M-steel materials.

2.4.3. FT-IR

We led to the realization of an infrared spectroscopy (FT-IR) analysis for a better study the MS surface following 6H of immersion in the corrosive HCl 1.0M solution in the absence and presence of inhibitors (ZB3 and ZB4).

2.5. Solution analysis

2.5.1. ICP-OES

Inductively coupled plasma (ICP) spectrometry has been explored to assess the elemental composition as well as the concentration of ions produced on mild-steel surfaces despite and in the presence of manufactured corrosion-inhibiting molecules. Mild steel samples were immersed in a solution of 1.0 M HCl alone (blank) and in a solution containing ZB3 & ZB4 for 48 h at 298 K.

2.6. Computational Details

2.6.1. DFT calculations

The Gaussian09 software was used for all calculations, this same quantum chemical computations were done with the DFT density functional theory to respect to the hybrid functional B3LYP, following the theorem of Kohn and Sham, and based on the three-parameter Becke function, combining the Hartree-Fock exchange contribution with non-local adjustment for the exchange potential put out by Becke [15] and the non-local correction for the energy correlation offered by Lee et al [16]. Theoretical study of the studied quinazoline-based molecules was performed in gas and aqueous phase by DFT/B3LYP with the 6-31++G(d,p) basis set, the energies of HOMO, LUMO orbitals and the gap (EHOMO - ELUMO) are also deduced from the most stable conformations of the studied molecules in their ground state. Thus, the ionization potential I and the electronic affinity A Were outlined in terms of E_{HOMO}, E_{LUMO} according to the Koopmans' theorem, as follows:

$$I = -E_{HOMO} \quad (3)$$

$$A = -E_{LUMO} \quad (4)$$

The calculated values of the I & A parameters may be employed to establish the values of absolute electronegativity ‘χ’, softness ‘σ’ (the inverse of hardness) , & absolute hardness ‘η’, through the following expressions [17]:

$$\chi = (I + A)/2 \quad (5)$$

$$\eta = (I - A)/2 \quad (6)$$

In addition, the rate of charge transfer (ΔN), According to the Pearson electronegativity scale, the following was determined for a reaction between 2 systems that have various electronegativities [17].

$$\Delta N = \frac{\chi_{Fe} - \chi_{inh}}{2(\eta_{Fe} + \eta_{inh})} \quad (7)$$

$$\Delta E_{\text{back-donation}} = -\eta/4 \quad (8)$$

Where χFe and χinh stand for the absolute electronegativity of iron and the inhibitory molecule, respectively. The absolute hardness of iron as well as the inhibitor molecule are represented by the symbols ηFe and ηinh.

2.6.2. MC simulation

In our paper, MC simulation was performed using COMPASS force field run in the powerful software (Materials Studio version 8.0) [18], to determine the stable configurations of all examined complexes and the molecular descriptors. Prior to the MC simulation, the inhibitor molecules are optimized using the Gaussian09 software with the DFT/B3LYP/6-31++G(d,p) level. For the MC simulation, the adsorption of quinazoline derivatives products on the iron surface, Fe(110) in the simulated aqueous medium ($400H_2O$, $50H_3O^+$, $50Cl^-$ and 1 inhibitor molecule studied) is approximated using the Adsorption Locator module, with the periodic conditions using an iron unit cell, cleaved at (h = 1, k =1 and l = 0) and the supercell (8×8×8) in the simulation box of size a = 40 Å, b = 40 Å and c = 0 Å and void 40 Å.

3. RESULTS AND DISCUSSION

3.1. Chemical part

The synthesis and characterization of the two products ZB3 and ZB4 are described in greater detail in the work by El Hajri et al [13].

3.2. Electrochemical part

3.2.1. Polarization plots

Figure 2 displays the I-E curves for M-S in 1.0M HCl at 298K without and with the presence of ZB3 and ZB4 at concentrations varied between 10^{-3} M and 10^{-6} M. The electrochemical parameters such as E_{corr}, β_c, β_a and the efficiency η_{PP} are presented in Table 1.

A modification on the cathodic and anodic polarization branches is noticed, which results from the existence of ZB3 and ZB4 species in the aggressive environment, this affects the corrosion potential "E_{corr}" towards more positive potentials. This outcome suggests that while the adding of these organic substances slows down the anodic dissolve of M-S. The curves of the cathodic domain have an exponential shape with parallel lines with the rise of inhibitor

amounts, which signifies that the reduction of H^+ protons on the metal surface is executed by the charge transfer process [19].

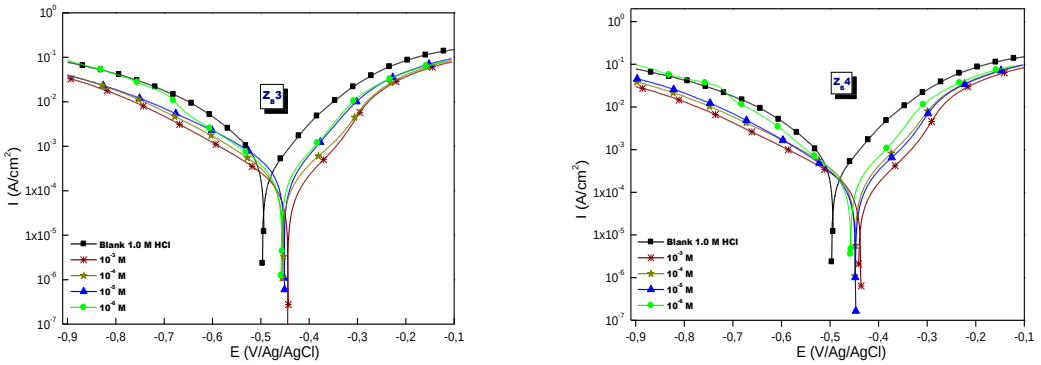

Figure 2. Polarization graphs for m-steel reprogrammed at 298 K in the studied environment prior to and following the inclusion of various amounts of ZB3 and ZB4

Table 1. Electrochemical characteristics for M-S measured at 298 K before and after adding varied amounts of the researched inhibitors to the media under investigation

Compounds	**Conc. M**	**E_{corr} mV/**	**i_{corr} µA cm^{-2}**	**- β_c mV dec^{-1}**	**β_a mV dec^{-1}**	**η_{PP} %**
HCl 1.0 M	--	-498	983	140	150	---------
Z_B3	10-3	-443	129	129	104	86.87
	10-4	-452	157	131	109	84.02
	10-5	-450	299	135	119	69.58
	10-6	-456	310	138	121	68.8
Z_B4	10-3	-436	133	128	103	86.46
	10-4	-447	171	136	108	82.60
	10-5	-446	213	135	110	78.33
	10-6	-456	263	122	113	73.24

Thus, it is apparent that the MS E_{corr} values in the table decline in absolute value when (ZB3 and ZB4) concentrations rise, however, in comparison to the corrosion potential of the free mixture, these values are lower than ±85 mV, this means that both compounds ZB3 and ZB4 are mixed-type inhibitors that prevent the anodic and cathodic processes directly implicated in the mild steel's corrosion in 1.0 M HCl [20,21].

With an increase in inhibitor concentration, the i_{corr} values drastically decline. Hence, as inhibitor concentration is increased, the inhibitory efficiency "η_{pp}%" rises as well, peaking at 86.87% and 86.46% for ZB3 and ZB4, respectively. This result suggests that both products adsorb efficiently onto the active sites present on the metal surface forming a protective film that minimizes its dissolution reactivity [22].

3.2.2. Electrochemical impedance spectroscopy

To ascertain and gather data about the protection mechanism (charge transfer, diffusion & adsorption) [23], EIS measurements were performed. The electrochemical properties of M-S in '1.0M HCl' at 298 K in the absence and existence of various concentrations of both products (ZB3 and ZB4) are shown in Figure 3 and 5 as Nyquist and Bode curves.

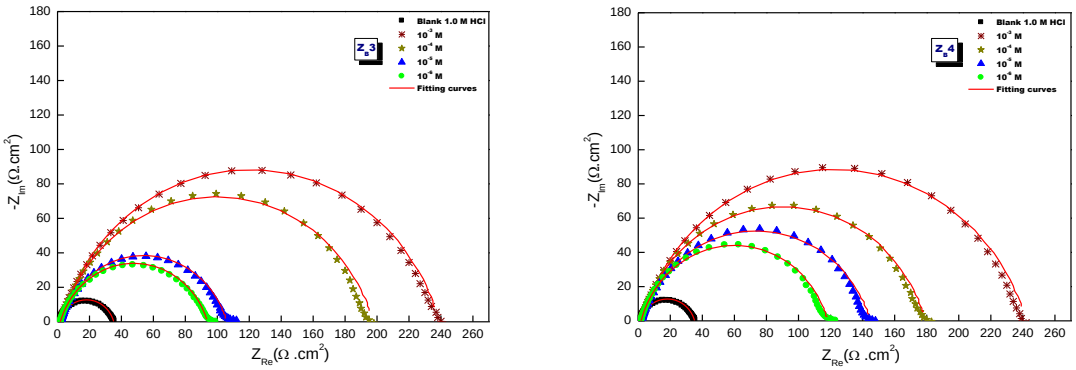

Figure 3. Nyquist impedance graphs for MS generated in HCl '1 M' at 298 K full of various inhibitor concentrations

It is noted that there is a single capacitive loop in all the graphs, which demonstrates that the corrosion reaction is primarily controlled by the charge transfer process [24]. The diameter of the capacitive loop widens with increasing amounts of the substances being investigated, which is consistent with the creation of a blocking layer on the mild-steel surface. However, these spectra show a similar shape over all concentrations tested, revealing that there is a formation of a thin film without changing the properties or corrosion mechanism [25]. The obtained Nyquist spectra show imperfect semicircles. This is probably due to electrode surface roughness or other non-uniformities [26]. The diameter of the capacitive loop grows with greater concentration, as shown by the Nyquist plots in the case of the presence of ZB3 and ZB4. This outcome may be linked to the increased creation of the preventative surface layer of inhibitor molecules on the mild steel surface and that the control potential of both inhibitors is related to its concentration in the film.

The model that has been chosen to simulate the Niquist diagrams is presented in Figure 4, (equivalent circuit). Solution resistance (R_s), parallel constant phase element (CPE) ((Q_{dl}, n_{dl}) or (C_{dl}, n_{dl})), and a charge transfer resistance made up this electrical circuit (R_{ct}). As a result, all experimental data were well-fit in both the existence and absence of quinazoline derivatives. The expression denotes the impedance function of the CPE [27]:

$$Z_{CPE} = 1/Q\ (j\ \omega)^{-ndl} \qquad (18)$$

Where Q represents the CPE's magnitude, j stands for an imaginary number (j2 = -1), and w represents the angular frequency. Ndl, the deflection parameter, denotes a phase shift (-1 ≤ ndl ≤+1). The CPE stands for a pure resistor if ndl = 0, an inductor if ndl = 1, & a pure capacitor if

ndl = 1. Moreover, the following equation has been used to determine the double-layer capacitances, Cdl, for a circuit that incorporates a CPE [27]:

$$C_{dl} = Q\,(2\pi\omega_{max})^{ndl-1} \quad (19)$$

where ω_{max} ($\omega_{max} = 2\pi f_{max}$) & f_{max} is to be the frequency at the highest value of the imagined section of the impedance profile.

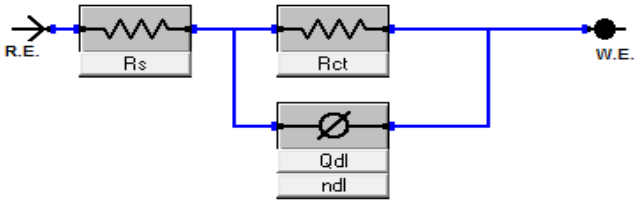

Figure 4. EEC applied to generate the experimental EIS data

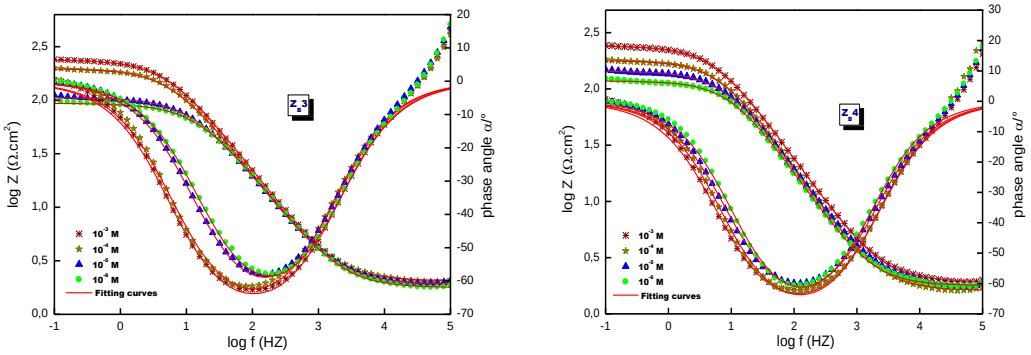

Figure 5. Bode diagrams of m-steel in 1 M HCl containing and omitting various concentration levels of ZB3 & ZB4 at 298 K

Table 2. Electrochemical impedance parameters for the inhibitory activity of M-S determined at 298 K in '1 M' HCl solution before and after adding various quantities of ZB3 and ZB4

Compounds	Conc. M	R_s (Ω cm²)	R_{ct} (Ω cm²)	Q (μF.S^{n-1})	n_{dl}	Θ	η_{imp} %
HCl 1.0M	--	1.12	34.7	419	0.773	-	-
Z_B3	10-3	1.926	237	235	0.815	0.8535	85.35
	10-4	2.051	195.5	259	0.813	0.8225	82.35
	10-5	1.922	104.1	270	0.810	0.6666	66.66
	10-6	1.770	92	264	0.809	0.6228	62.28
Z_B4	10-3	1.919	240.2	226	0.810	0.8555	85.55
	10-4	1.610	177.6	250	0.808	0.8046	80.46
	10-5	1.776	143.2	286	0.806	0.7576	75.76
	10-6	1.777	116.5	272	0.803	0.7021	70.21

The EIS test results are displayed as Bode angle graphs, which make reference to an equivalent circuit with a singular constant phase element at the contact between the metal and the environment. Phase angle and Bode diagrams increase as the concentration of the molecules increases. This indicates that the protecting capacity is proportional to the adsorption capacity of the inhibitor particles on the mild-steel surface [28].

Table 2 shows the electrochemical parameter values, including R_s, R_{ct}, Q, n_{dl}, and η_{imp}(%) related to the two products ZB3 and ZB4. It is noted that the R_{ct} values increase with increasing concentration reaching maximum values of 237 Ω cm^2 and 240.2 Ω cm^2 for ZB3 and ZB4, respectively. Whereas, the n_{dl} values are higher than the free solution value and enlarge with increasing concentration. This result indicates that those inhibitors are thoroughly adsorbing to the steel surface, where they create a shielding coating [29,30].

The inhibitory efficacy of both compounds increases proportionally with concentrations ranging from 62.28% to 85.35% for ZB3 and 70.21% to 85.55% for ZB4. It is noted that both inhibitors have the same inhibitory efficiency which suggests that the addition of a second chlorine function has no effect on the performance of the molecules examined.

3.3. Adsorption isotherm

In order to explore the inhibitors' adsorption characteristics on metallic surfaces in an acidic environment, many types of adsorption isotherms are tested such as (Langmuir's isotherm, Temkin, Frumkin, etc.) [31]. The criterion for selecting the best adsorption isotherm was the value of the regression coefficient (R^2) that was closest to unity for the Langmuir adsorption isotherm model. The Langmuir adsorption isotherm is given as follows [32]:

$$\frac{Cinh}{\theta} = \frac{1}{Kads} + Cinh \quad (21)$$

where, C_{inh} denotes the inhibitor concentration (ZB3 and ZB4), K_{ads} is the adsorption-desorption equilibrium constant and θ is the surface coverage with ($\theta = \eta_{PP}/100$). The plot of Langmuir adsorption isotherm (C_{inh}/θ vs. C_{inh}) for corrosion of mild-steel in an environment of '1 M' HCl is presented in Figure 6. The regression coefficient values (R^2 = 1 for ZB3 & 0.99998 for ZB4), which validates the suitability of this approach. Using K_{ads}, the values of the "$\Delta G_{ads}°$" were determined by applying the equation that follows [33] (Table 3):

$$\Delta Gads = -RT \ln (55.5 * Kads) \quad (22)$$

where R: is the universal gas constant,

55.55: concentration of water in solution (mol L^{-1}),

T: absolute temperature (K),

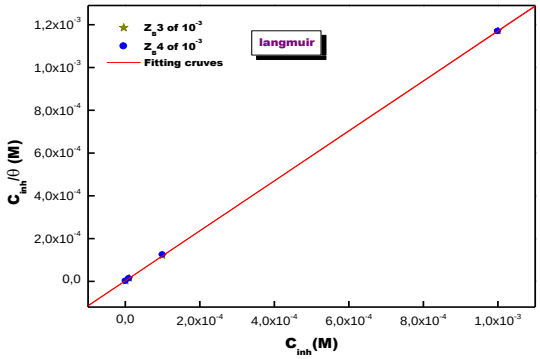

Figure 6. Langmuir adsorption curves for different quinazolinone derivatives on mild steel in '1.0 M' HCl media at 298 K

Table 3. Thermodynamic parameters obtained for the adsorption of ZB3 and ZB4 on M-S in '1.0 M' HCl at 298 K by the use of the Langmuir adsorption isotherm

Inhibiteurs testés	**K_{ads} (L/mol)**	**R^2**	**ΔG_{ads} (Kj/mol)**
Z_B3	364920.88	1	-41.66
Z_B4	333483.40	0.9999	-41.43

The fact that the Gads values are negative indicates that the inhibition is being adsorbed spontaneously. It is widely known that the adsorption of organic compounds to the surface of steel is measured using the two primary types of adsorption, physisorption and chemisorption. However, if the value of ΔG_{ads} is equal to or less than -20 kJ /mol, it could be inferred that physisorption is the form of adsorption, in which charged inhibitor molecules interact electrostatically with the metal. If the ΔG_{ads} value is equal to or greater than -40 kJ /mol, the nature of adsorption is still referred to chemisorption and the process is able to be clarified through charge sharing or transfer of electrons from the inhibitor products to the ferrous atoms [34]. The ΔG_{ads} values obtained in our case are close to -40 kJ/moL, which proves that the ZB3 and ZB4 compounds could really spontaneously interact with iron by chemical adsorption.

3.3. Activation parameters and temperature effect

The influence of temperature on the corrosion rate of M-steel in 1 M HCl in the absence and presence of 10^{-3} of ZB3 and ZB4 was studied at different temperatures ranging from 298 to 328K. The curves and polarization parameters obtained in this study are presented in Figure 1 supplementary and Table 4, respectively.

Table 4. PP parameters of M-S in 1 M HCl containing '10^{-3} M' of ZB3 & ZB4 at varying temp

Compounds	Temperature K	E_{corr} mV_{SCE}	i_{corr} $\mu A\ cm^{-2}$	$-\beta c$ $mV\ dec^{-1}$	β_α $mV\ dec^{-1}$	η_{imp} %
Blank	298	-498	983	140	150	----
	308	-477	1200	184	112	----
	318	-487	1450	171	124	----
	328	-493	2200	161	118	----
Z_B3	298	-443	129	129	104	86.87
	308	-442	372	143	126	69.00
	318	-448	458	153	131	68.41
	328	-464	744	161	116	66.18
Z_B4	298	-436	133	128	103	86.46
	308	-458	316	154	113	73.66
	318	-452	470	164	125	67.58
	328	-475	730	144	118	66.81

It is observed that the current densities increase with increasing temperature for mild steel material in 1 M HCl containing and without the addition of inhibitors. The accelerated chemical processes can account for these outcomes, this implies that mild steel's rate of corrosion is influenced by temperature [35]. The effectiveness of both products' inhibitors decreases with increasing temperature, which reveals chemical adsorption or the presence of weak chemical bonds between the inhibitor molecules and the steel surface [36].

Kinetic and thermodynamic characteristics, particularly apparent activation energy (E_a), activation enthalpy (ΔH_a), and activation entropy (ΔS_a) for the dissolution of mild steel in 1M HCl both when absent then when present of 10^{-3}M ZB3 and ZB4 at 298-328 K are presented in Figure 2 supplementary and Table 5. The Arrhenius equation served as the basis for the calculation of the activation parameters [37]:

$$i_{corr} = Ae^{-Ea/RT} \quad (23)$$

We obtain the following when we take the logarithm from both sides of the Arrhenius equation:

$$\text{Ln } i_{corr} = \text{Ln } A - Ea/RT \quad (24)$$

The transition state equation was used to determine the variation in enthalpy {ΔHa} & entropy {ΔSa} for the production of the activated complex in the state of transition [37]:

$$\ln\left(\frac{icorr}{T}\right) = \left[\ln\left(\frac{R}{hNa}\right) + \left(\frac{\Delta Sa}{R}\right)\right] - \Delta Ha/RT \quad (25)$$

where

i_{corr} : Corrosion current density,

A : Pre-exponential factor,

h : Planck's constant,

Na : Avogadro's number,

Ea : Apparent activation energy,

R : Gas constant (R = 8.314 J mol^{-1}. K^{-1})

T : Absolute temperature.

A plot of ln (i_{corr}) versus 1000/T shown in Figure 2 supplementary shows a straight line with a slope of the line ($-E_a/R$). E_a values are been determined by the slope and are shown in Table 5.

Table 5. Activation parameters for m-steel in 1 M HCl solution in the absence and presence of ZB3 & ZB4 inhibitors

	E_a (KJ/mol)	**ΔH_a (KJ/mol)**	**ΔS_a (J/mol.K)**
Blanc	21.0	18.5	-126.0
Z_B3	45.28	42.71	-60.0
Z_B4	44.87	42.29	-61.41

It is noted that the E_a values of the solution containing 10^{-3} M of ZB3 and ZB4 are higher than those of the uninhibited solution, this can be interpreted by the physical adsorption of the two molecules on the surface. The development of a thin barrier film on the mild steel's surface is responsible for these communications. The higher energy barrier for the corrosion process in the inhibited solutions indicates that the adsorbed inhibitor coating stops the charge/mass transfer reaction from happening on the surface and hence guards the metal against oxidation. [38,39].

The table also shows that the activation enthalpy values (ΔH_a) obtained in the presence of both compounds are higher than that of the free solution, indicating that the corrosion process between the compounds (ZB3 & ZB4) and (Fe: iron) in an acidic environment is endothermic [40]. In addition, it is noted that the values of entropies (ΔS_a) increase negatively after the addition of ZB3 and ZB4, showing less desorganized behavior owing to the complex being active during the rate-setting phase.

3.3. Surface analysis

3.3.1. SEM/EDX

The surface morphologies of mild steel after immersion in 1 M HCl solution for 6H before and after the addition of 10^{-3} M of ZB3 and ZB4 inhibitors were obtained by SEM. The steel

not allowed to be treated with the solution which contain the two products (Figure 3 supplementary (BLK)) was severely damaged and became rough due to the attack of the aggressive solution. However, as shown in Figure 3 supplementary (ZB3, ZB4), a less corroded and smoother surface was clearly observed on the iron samples treated with the film-forming solution of ZB3 and ZB4, respectively. These results indicate that the effective adsorption of these quinazoline derivatives on the surface of mild steel could significantly limit the corrosive attack.

Table 6. Compositions of the m-steel surface tested by EDS analysis

Elements	Blank	ZB3	ZB4
C	4.52	4.27	2.84
O	27.86	24.73	6.91
Fe	67.62	69.78	90.26
Cl	1.04	1.03	--
Si	0.35	--	--

EDS analysis was applied to further confirm the elemental composition of the film deposited on the steel surface [41]. Figure 4 supplementary performs the peaks obtained for the elements C, O, Cl, and Fe present on the surface of the sample before and after 6h soaking in 1 M HCl containing 10^{-3} M ZB3 and ZB4. The percentage of the different elements detected on the steel electrode is listed in Table 6.

The spectra related to ZB3 and ZB4 show a remarkable reduction in the signal corresponding to C and O compared to that of the blank, while the % of Fe increases. This suggests that quinazolinone derivatives are well adsorbed just on the metallic surface forming a barrier layer resistant to the aggressive corrosive environment [42].

3.3.2. FT-IR analysis

Fourier transform infrared spectroscopy (FTIR) analysis was adopted to investigate the compositional changes that occurred after 6H immersion of mild steel in 1 M HCl before and after the addition of the two inhibitors ZB3 and ZB4 [43] (Figure 5 supplementary).

The FT-IR spectrum corresponding to the solution containing the film-forming solution of ZB3 and ZB4 shows the appearance of several peaks with different wavenumbers related to the existence of the examined inhibitors. However, the absence of these molecules reveals the disappearance of these peaks. This result explains the inhibitors' adsorption by producing a shield on the MS surface.

3.3.3. Structural analysis (X-ray diffraction analysis)

The diffractograms obtained using the XRD technique and associated with the analysis of the steel surface after 6H of immersion in 1 M HCl solution before and after the addition of ZB3 and ZB4 are presented in Figure 6 supplementary.

The results obtained for the blank solution demonstrate the presence of Fe_3O_4 and Fe_2O_3 (iron oxides) peaks, which can be recognized at θ= 29.40° and 65°, respectively. Nevertheless, the Fe_3O_4-related peak disappeared completely, while the intensity of the Fe_2O_3-related peak decreased for solutions containing the species examined, indicating that the mild steel surface had been isolated and protected from the aggressive solution by a protective layer.

3.4. Solution analysis

By using ICP-OES, it is possible to accurately detect the elemental composition and concentration of dissolved iron ions in both inhibited and uninhibited mixtures. Table 7 shows the concentration values of 'Fe^{2+}' ions present in 1 M HCl alone and after the addition of different concentrations of ZB3 & ZB4.

Table 7. Concentration of Fe^{2+} ions in 1 M HCl without & with the presence of various quantities of ZB3 & ZB4

Compounds	**Conc. M**	**Conc Fe^{2+} Ions mg/L**
HCl 1 M	--	1152
ZB3	10^{-3}	236.5
	10^{-4}	293.2
	10^{-5}	403.0
	10^{-6}	514.1
ZB4	10^{-3}	175.9
	10^{-4}	274.9
	10^{-5}	304.5
	10^{-6}	398.0

The results obtained show that the concentration of Fe^{2+} ions in solution decreases (1152 mg/L for the Control) as the inhibitor concentration increases from 514.1 to 236.5 mg/L for a concentration ranging from 10^{-6} to 10^{-3} M, for ZB3. The same is true for ZB4; as the concentration increases from 10^{-6} to 10^{-3} M, the quantity of Fe^{2+} ions in the solution decreases from 398.0 to 175.9 mg/L.

These results indicate that steel dissolution is rapidly inhibited in the presence of the inhibitors studied.

3.5. DFT Calculations

3.5.1. Structural analysis

For a better understanding of the evolution of intrinsic reactivity descriptors and their possible correlation with the inhibitory efficacy of the inhibitors studied, we proceeded by studying the effect of the substitution of the hydrogen atom in positions 13 and 17 in the quinazolinone derivative by a chlorine atom on the corresponding inhibitory efficiencies. To this end, we carried out a theoretical study on 2-(4-chlorophenyl)-2,3-dihydroquinazolin-4(1H)-one (ZB3) and 2-(2,4-dichlorophenyl)-2,3-dihydroquinazolin-4(1H)-one (ZB4) (Figure 7 supplementary) both in isolated state and in solution (PCM with a ε=78.93) at the same DFT(B3LYP)/6-31G(d,p) level.

The optimized geometries of ZB3 and ZB4 molecules are shown in (Figure 7 supplementary), and the values for bond length and bond angle in the molecules studied are presented in Table 8.

The [C7-N1-C2-C12] dihedral angle values for two inhibitors, ZB3 and ZB4, are of the order of 171.22° and 170.43° respectively. The dihedral angles [N3-C2-C12-C14] for the two compounds ZB3 and ZB4 are of the order of 61.53° and 61.00°, respectively. This shows the non-planarity of the inhibitors under study, a result proved by the nature of the carbon (C2), which is of the SP^3 hybridization. Also, the values of the dihedral angle [C7-C6-C4-O5] for the same inhibitors are 172.48° and 172.81° respectively. This result shows the existence of planarity in the quinazolinone derivative, proving a delocalization of π electrons in the quinazolinone group of these molecules.

We also note that the values of the dihedral angles [C14-C16-C17-Cl18/Cl19] of two inhibitors are of the order of 179.97° and 179.97° respectively, ZB3 and ZB4. The dihedral angle [C2-C12-C13-Cl18] of the ZB4 molecule is of the order of 0.10°. This result shows that chlorine atoms (Cl18 and Cl19) can contribute to electron delocalization in the two inhibitors studied.

The analysis of bond length values shows that: C7-N1, N1-C2, C2-N3 and N3-C4 in the quinazolinone fragment are respectively [1.395, 1.461, 1.461 and 1.384 Å for the ZB3 molecule] and [1.397,1.463, 1.462 and 1.386 Å for the ZB4 molecule] in the gas phase, these bond lengths being homologous with the C-N bond lengths reported in the following references [44,45]. As well, the C-C bond lengths of the benzene ring of two compounds are between 1.392 and 1.401 Å. However, it can be seen that the benzene ring comprises C-C bond lengths varying between double bond lengths and single bond lengths [46]. These intermediate bond length values obtained in this study show that bond conjugation occurs in the benzene rings of

two inhibitors, reinforcing the strong π-electron delocalization in the quinazolinone derivative of all molecules.

Table 8. The geometrical properties of the investigated inhibitors were computed at B3LYP/6-31G(d,p) in the gaseous (G) and aqueous (A) phases

Phase	Distance en (Å)	ZB3	ZB4	Angle dièdre en (°)	ZB3	ZB4
G	**N_1-C_7**	1.395	1.397	**[C_7-C_6-C_4-O_5]**	172.48	172.81
A		1.391	1.392		171.02	170.98
G	**C_6-C_7**	1.411	1.411	**[O_5-C_4-N_3-C_2]**	160.60	160.20
A		1.413	1.413		162.66	162.66
G	**C_4-C_6**	1.485	1.485	**[C_7-N_1-C_2-C_{12}]**	171.22	170.43
A		1.483	1.483		170.85	170.27
G	**C_4-O_5**	1.225	1.225	**[C_2-C_{12}-C_{13}-C_{15}]**	179.92	179.96
A		1.234	1.233		179.88	179.34
G	**C_4-N_3**	1.384	1.386	**[C_2-C_{12}-C_{14}-C_{16}]**	179.96	179.97
A		1.374	1.374		179.89	179.38
G	**N_3-C_2**	1.461	1.462	**[C_9-C_7-N_1-C_2]**	153.50	153.20
A		1.466	1.466		153.40	153.12
G	**N_1-C_2**	1.461	1.463	**[C_8-C_6-C_4-N_3]**	178.17	178.25
A		1.461	1.462		177.33	177.23
G	**C_2-C_{12}**	1.516	1.519	**[N_3-C_2-C_{12}-C_{14}]**	61.53 61.85	61.00
A		1.516	1.519			68.45
G	**C_7-C_9**	1.404	1.403	**[N_3-C_2-C_{12}-C_{13}]**	118.38	118.90
A		1.406	1.405		118.03	110.53
G	**C_6-C_8**	1.398	1.398	**[N_1-C_2-C_{12}-C_{13}]**	123.18	123.54
A		1.400	1.400		123.53	131.55
G	**C_9-C_{11}**	1.391	1.391	**[C_9-C_7-C_6-C_4]**	176.66	176.95
A		1.391	1.391		176.25	176.40
G	**C_8-C_{10}**	1.390	1.391	**[C_{14}-C_{16}-C_{17}-**	179.97	179.97
A		1.390	1.390	**Cl_{18}/Cl_{19}]**	179.99	180.00
G	**C_{10}-C_{11}**	1.400	1.400	**[C_2-C_{12}-C_{13}-Cl_{18}]**	----	0.10
A		1.402	1.402		----	0.51
G	**C_{12}-C_{13}**	1.396	1.400			
A		1.516	1.400			
G	**C_{12}-C_{14}**	1.401	1.403			
A		1.401	1.402			
G	**C_{13}-C_{15}**	1.396	1.397			
A		1.396	1.396			
G	**C_{14}-C_{16}**	1.392	1.390			
A		1.393	1.391			
G	**C_{15}-C_{17}**	1.393	1.391			
A		1.392	1.391			
G	**C_{16}-C_{17}**	1.397	1.396			
A		1.396	1.394			
G	**C_{13}/C_{17}-Cl_{18}**	1.757	1.763			
A		1.764	1.764			
G	**C_{17}-Cl_{19}**	----	1.753			
A		----	1.758			

We noted that the C13-Cl18 and C17-Cl18 bond lengths show values of (1.757 and 1.763 Å) for ZB3 and ZB4, respectively. Thus, the bond length (C17-Cl19 1.753 Å) in the ZB4 molecule, this result is clearly similar to the normal value for this double bond in the literature

[47]. Such findings illustrate the high polarizability of the C-Cl bond in the inhibitors studied, which may explain the adsorption of these molecules to the mild-steel surface via these chlorine atoms. Furthermore, the solvent effect affects neither the flatness nor the structural parameters of the quinazolinone derivatives.

3.5.2. Study of global reactivity descriptors

The values of the various intrinsic properties of ZB3 and ZB4 that were determined at the DFT level (B3LYP)/6-31G(d,p) in both the isolation state and in solution are listed in Table 9.

In order to investigate the reactivity of the systems studied, the frontier orbitals describe the best reactivity of the molecular systems within the framework of Fukui's theory [48], according to which the highest occupied orbital's energy (HOMO) presents the capacity of the molecular systems to donate electrons. Whereas that of the lowest vacant orbital (LUMO) presents the disposition of molecular systems to receive electrons.

Table 9. Examined inhibitors' quantum chemical descriptors measured at B3LYP/6-31G(d,p) level of theory in both gas and in aqueous

Inhibitor / Descriptor	ZB3		ZB4	
	gas	**aqueous**	**gas**	**aqueous**
E_{Total} **/ a.u**	-1185.080843	-1185.094225	-1644.670247	-1644.682953
E_{HOMO} **/ eV**	-5.845	-5.822	-5.900	-5.862
E_{LUMO} **/ eV**	-1.089	-1.147	-1.278	-1.209
ΔE **/ eV**	4.756	4.675	4.622	4.653
μ **/ D**	3.970	5.538	3.698	5.399
I **/ eV**	5.845	5.822	5.900	5.862
A **/ eV**	1.089	1.147	1.278	1.209
χ **/ eV**	3.467	3.484	3.589	3.536
η **/ eV**	2.378	2.337	2.311	2.326
σ **/ eV^{-1}**	0.421	0.428	0.433	0.430
ΔN	0.743	0.752	0.738	0.745
$\Delta E_{\text{back-donation}}$ **/ eV**	-0.595	-0.584	-0.578	-0.582

The boundary orbital energy values of the two quinazolinone derivatives (Table 9) show that in the isolated state, the HOMO of ZB3 is slightly higher than that of ZB4. We also note that the LUMO of ZB4 is slightly lower than that of ZB3. In fact, when we analyze the type of these products reactivity's, we note that the slight electrophilic reactivity (low LUMO) of ZB3 is offset by their elevated nucleophilic reactivity (high EHOMO). This contrasts with ZB4,

where a slight deficit in nucleophilic reactivity (high MWLE) is offset by their electrophilic reactivity (low MWOE).

Furthermore, a system is all the more reactive if it has the availability to give up and accept electrons, hence the importance of the energy gap ΔE between the frontier orbitals of the same system. Molecules with a small gap are generally more reactive [49]. The ΔE values of the two quinazolinone derivatives (Table 9) show that ZB4 has the smaller Gap (4.622 eV) compared to that of ZB3 (4.756 eV); this would probably confer a better reactivity to ZB4.

Calculation of the dipole moment μ of quinazolinone derivatives reflects the charge distribution over the entire molecule. A high value of dipole moment reflects better reactivity, particularly in the case of electrostatic reaction [50]. According to the μ values of ZB3 and ZB4 (Table 9), the dipole moment values of two inhibitors are similar, giving the latter a better reactivity [51].

It can also be seen from the electronegativity χ results given in Table 9 that ZB4 exhibits a slightly elevated value compared to that of ZB3. Given that electronegativity is a measure of a system's capacity to draw electrons to itself (atomic or molecular), it may have been concluded that ZB4 might exhibit a slightly higher electron acceptor behavior from the metal surface than ZB3, which is consistent with previous findings of LUMO molecular orbital energy values. On the other hand, the values of softness σ (inverse of hardness η) also attest to the high reactivity of ZB3 and ZB4 compared with that published in the literature [52]. What's more, the values of the back-donation energetics ($\Delta E_{back\text{-}donation}$) seem to have been negative across both cases, denoting an energetically favorite back-donation of quinazolinone derivatives to the metal surface. Thus, this finding also corroborates the results obtained by preceding quantum chemical parameters.

The global reactivity descriptors previously discussed are used to analyze the intrinsic reactivity of a molecule without involving the material. However, the charge transfer rate ΔN has the particularity of involving both reactants; the inhibitor and the metal, in the reactivity analysis, as shown by its expression (3.7).

Analysis of ΔN values (Table 9) shows that all values are positive; indicating that charge transfer flow is probably from the inhibitor to the metal.

Overall, the results of the global reactivity descriptors for ZB3 and ZB4 suggest that these molecules possess the appropriate electronic properties of good corrosion inhibitors, with a remarkable corrosion-inhibiting efficacy found experimentally.

3.5.3. Electron density distributions of border orbitals and MEP maps of ZB3 and ZB4 inhibitors

In order to explain the adsorption process of inhibitors on the metal surface through charge transfer, which is generated from the highest occupied molecular orbitals (HOMOs) to the lowest unoccupied molecular orbitals (LUMOs) [53], the selected FMOs of all the inhibitors studied are shown in Figure 8 supplementary. An evaluation of the electron densities of both

the HOMO and LUMO frontier orbitals of ZB3 and ZB4 shown in Figure 8 supplementary indicates that the two molecules have almost identical FMO distributions. The HOMO orbital distributions of both inhibitors are mainly distributed over the entire quinazolinone moiety of these inhibitors; this reflects the electronic conjugation of the quinazolinone ring, and the LUMO orbital distributions of both inhibitors are fairly evenly distributed over the entire molecule. These results show that these molecules have a high affinity for receiving electrons from the metal. Consequently, this result suggests that the quinazolinone moiety represents the most likely potential sites on the metal surface. These data can be supported and affirmed by the adsorption modes obtained by Monte Carlo simulations in the next section of this work.
Molecular electrostatic potential (MEP) simulation using the B3LYP/6-31G(d,p) level of quinazolinone derivatives, shown in Figure 8 supplementary, is used to predict the reactive regions of the molecules studied under electrophilic and nucleophilic attack. On the MEP surface, various electrostatic potential levels are depicted by various colors. Positive, negative and neutral regions are represented by blue, red and green colors respectively [54].

It can be seen that the red-to-green zone can be recognized to be ideal for electrophilic attack, especially detected on the quinazolinone moiety of the two inhibitors studied. In addition, a region from green to blue is equivalent to the zone sensitive to nucleophilic attack, which covers the entire part of the molecules, except for the quinazolinone group region, while the absence of potential is expressed by the color green.

3.5.4. Local molecular selectivity

To examine the selectivity of the systems studied, we calculated the natural populations of atoms in the different species: neutral, cationic, and anionic. In order to analyze descriptors of the local reactivity of these inhibitors, Fukui indices in particular would be the approach of choice for identifying the most reactive sites in the systems studied [55].

Analysis of the Fukui index values of the two quinazolinone-derived inhibitors (Figure 9 supplementary and Table 10) shows that both inhibitors have three nucleophilically attackable centers (electrophilic centers) with high f_k^+ values, C4, O5, and C11. The results also show that these two inhibitors also feature four sites with high f_k^- values, N1, C6, C9, and C10, making these atoms locations vulnerable to electrophilic attack (nucleophilic centers).

It's crucial to underline that, examining these two molecules ZB3 and ZB4 shows, the emergence of N1 and C10 atoms in terms of a nucleophilic character, with a nucleophilic power more pronounced on the nitrogen atom with the highest f_k^- values calculated in the isolated state are of the order of 0.217 and 0.214 for ZB3 for ZB4, respectively; such behavior would result from the availability of nitrogen orbitals in ZB3/ZB4. We also note that this site may show a more pronounced commitment to reactivity as a nucleophilic center in the inhibitors studied. This would offer this site a greater capacity for adsorption on the metal surface than the other reactive sites, notably given that the nitrogen atom has the highest f_k-value.

Table 10. Relevant natural populations and ZB1 and ZB2 Fukui functions computed at B3LYP/6-31G(d,p) in the gas, G, and aqueous, A phases

		ZB3					ZB4				
Atom	**Phase**	P_N	P_{N-1}	P_{N+1}	f_k^+	f_k^-	P_N	P_{N-1}	P_{N+1}	f_k^+	f_k^-
N_1	G	7.648	7.442	7.657	0.009	0.217	7.651	7.437	7.655	0.004	0.214
	A	7.651	7.422	7.677	0.026	0.240	7.654	7.424	7.677	0.023	0.229
C_2	G	5.870	5.878	5.890	0.021	-0.007	5.875	5.882	5.899	0.024	-0.006
	A	5.871	5.879	5.882	0.011	-0.007	5.874	5.880	5.889	0.016	-0.001
N_3	G	7.683	7.667	7.702	0.019	0.022	7.686	7.669	7.695	0.009	0.017
	A	7.673	7.647	7.727	0.054	0.031	7.674	7.649	7.726	0.052	0.025
C_4	G	5.311	5.326	5.393	0.081	-0.018	5.310	5.328	5.370	0.060	-0.018
	A	5.309	5.314	5.447	0.139	-0.009	5.308	5.313	5.443	0.135	-0.005
O_5	G	8.611	8.549	8.697	0.087	0.068	8.608	8.552	8.683	0.075	0.056
	A	8.665	8.623	8.775	0.109	0.048	8.662	8.619	8.768	0.106	0.043
C_6	G	6.199	6.112	6.234	0.035	0.092	6.199	6.115	6.222	0.023	0.084
	A	6.208	6.113	6.268	0.060	0.099	6.207	6.114	6.263	0.056	0.093
C_7	G	5.803	5.766	5.828	0.024	0.034	5.804	5.767	5.818	0.014	0.037
	A	5.799	5.754	5.846	0.047	0.040	5.799	5.753	5.846	0.047	0.047
C_8	G	6.171	6.173	6.220	0.049	-0.002	6.170	6.171	6.205	0.035	-0.001
	A	6.183	6.176	6.278	0.095	0.008	6.182	6.174	6.269	0.087	0.008
C_9	G	6.284	6.207	6.303	0.019	0.084	6.283	6.204	6.296	0.013	0.079
	A	6.285	6.187	6.327	0.043	0.103	6.284	6.187	6.320	0.037	0.097
C_{10}	G	6.272	6.115	6.287	0.015	0.168	6.271	6.117	6.291	0.020	0.154
	A	6.281	6.119	6.288	0.007	0.171	6.280	6.117	6.288	0.009	0.163
C_{11}	G	6.202	6.203	6.290	0.088	-0.002	6.201	6.204	6.266	0.065	-0.003
	A	6.205	6.208	6.333	0.128	-0.005	6.204	6.208	6.325	0.120	-0.003
C_{12}	G	6.083	6.124	6.115	0.032	-0.040	6.099	6.117	6.178	0.078	-0.017
	A	6.080	6.097	6.067	-0.014	-0.015	6.094	6.111	6.091	-0.003	-0.017
C_{13}	G	6.214	6.211	6.216	0.002	0.004	6.017	6.023	6.001	-0.015	-0.001
	A	6.208	6.201	6.216	0.008	0.007	6.012	6.012	6.013	0.001	0.001
C_{14}	G	6.202	6.206	6.259	0.057	-0.004	6.188	6.203	6.256	0.068	-0.015
	A	6.204	6.199	6.216	0.012	0.006	6.188	6.183	6.208	0.020	0.005
C_{15}	G	6.247	6.228	6.307	0.059	0.021	6.264	6.247	6.325	0.061	0.017
	A	6.250	6.242	6.261	0.012	0.008	6.264	6.256	6.282	0.018	0.008
C_{16}	G	6.246	6.231	6.258	0.013	0.017	6.250	6.228	6.263	0.013	0.022
	A	6.250	6.242	6.257	0.007	0.008	6.248	6.241	6.255	0.007	0.007
C_{17}	G	6.038	6.028	6.080	0.042	0.031	6.029	6.023	6.098	0.069	0.006
	A	6.040	6.033	6.049	0.009	0.014	6.029	6.022	6.044	0.015	0.007
Cl_{18}	G	----	----	----	----	----	16.992	16.980	17.065	0.073	0.012
	A	----	----	----	----	----	16.998	16.978	17.019	0.020	0.020
Cl_{19}	G	16.998	16.936	17076	0.078	----	16.985	16.925	17.074	0.089	0.060
	A	17.018	17.002	17.033	0.015	----	17.000	16.984	17.019	0.019	0.016

3.5.5. Natural Bond Orbitals NBO analysis

The NBO atomic charge values evaluated at the B3LYP/6-31G(d,p) level for quinazolinone-derived inhibitors are shown in Figure 10 supplementary and in Table 11, which similarly gathers the NBOs on the relevant atoms.

According to the inhibitors studied, the most pronounced sites of interaction for reactivity are oxygen (O) and nitrogen (N) atoms. Atomic charges computed for the two inhibitors in Figure 10 supplementary and Table 11 support this finding.

The highest negative charge values of the NBO atomic charges of these molecules are found for nitrogen (N1, N3) and oxygen (O5) atoms, consistent with adsorption sites via a donor-acceptor interaction. In addition, it implied to the existence of electron-oic delocalization

in quinazolinone derivatives, reflecting that the chemical compound's mesomeric action enhances its reactivity.

Table 11. Mulliken charge distribution for the neutral quinazolinone derivatives calculated at the B3LYP/6-31G(d,p) in gas and aqueous phases

Inhibitor / Atom	ZB3		ZB4	
	Gas	aqueous	Gas	aqueous
N_1	-0.600	-0.611	-0.601	-0.614
C_2	0.184	0.186	0.174	0.181
N_3	-0.558	-0.560	-0.559	-0.556
C_4	0.566	0.565	0.565	0.566
O_5	-0.515	-0.574	-0.513	-0.572
C_6	0.023	0.021	0.027	0.024
C_7	0.291	0.289	0.289	0.288
C_8	-0.118	-0.134	-0.118	-0.133
C_9	-0.127	-0.138	-0.127	-0.137
C_{10}	-0.099	-0.115	-0.098	-0.114
C_{11}	-0.084	-0.098	-0.084	-0.098
C_{12}	0.054	0.061	0.068	0.080
C_{13}	-0.123	-0.123	-0.149	-0.143
C_{14}	-0.089	-0.096	-0.083	-0.089
C_{15}	-0.074	-0.081	-0.057	-0.057
C_{16}	-0.073	-0.089	-0.078	-0.073
C_{17}	-0.092	-0.097	-0.090	-0.094
Cl_{18}	----	----	0.006	-0.003
Cl_{19}	-0.013	-0.039	0.002	-0.017

Consequently, it should be noted that the results obtained from the above quantum chemical parameter calculations do not directly reflect the trend obtained in inhibition performance, suggesting that they are not associated with the relative inhibition strengths of the quinazolinone derivatives studied.

3.6. MC simulation results

Monte Carlo simulation is an effective method for exploring and explaining the adsorption process. As a result, it was done to forecast the adsorption energies of inhibitors on the mild steel surface and to demonstrate if there is a notable correlation between adsorption energies

and experimental data for the inhibitors examined in this work. Resulting from what was found by electrochemical impedance spectroscopy analysis; both inhibitors are adsorbable to mild steel. Figure 11 supplementary shows the most stable adsorption configurations illustrated in both top and side views of ZB3 and ZB4 on a mild steel surface (110).

According to Figure 11 supplementary, the two molecules are adsorbed in different ways on the surface studied, the molecule ZB3 adsorbs in a vertical manner exposing through the benzene ring that carries the chlorine atom, this portion of the molecule will be responsible on adsorption and provide a coverage of the iron surface to block metal dissolution. Furthermore, the straight and parallel orientation of the ZB4 inhibitor on the metallic surface investigated will definitely provide a larger blocking surface for adsorption and, consequently, a higher adsorption capacity is observed for this molecule. This is consistent with the fact that the heteroatoms: (chlorine (Cl) and nitrogen (N)) and the benzene ring on the inhibitor have negative atomic charge values (NBO) Figure 11 supplementary. The shortest distances between molecules and surfaces are also demonstrated by the most persistent adsorption configurations, indicating that the adsorption process is chemical in nature. This outcome is consistent with the experimental information found by electrochemical impedance spectroscopy (EIS).
The calculated adsorption energies are shown in Table 12.

Table 12. MC simulation outcomes and descriptors for the adsorption of quinazolinone compounds on the Fe (110) surface (kcal.mol^{-1})

Ligand	E_{Total}	E_{Ads}	RAE	E_{Def}	$dE_{Ads}/dNi_{inhibitor}$	dE_{Ads}/dNi_{H2O}
ZB3	-636.94	-1569.44	-668.07	-901.37	-43.88	-1.55
ZB4	-643.38	-1579.06	-677.35	-901.71	-45.22	-1.41

Alternatively, the total energy (E_{Total}), adsorption energy (E_{Ads}), rigid adsorption energy (RAE), deformation energy (E_{Def}), $dE_{Ads}/dN_{iinhibitor}$ and dE_{Ads}/dN_{iH2O} are presented in Table 12. In fact, such energies might indicate how well the inhibitors investigated could adsorb to the surface of iron Fe (110) [56]. The theoretical study states that, in the simulation process, inhibition performance is higher when the adsorption energy is lower. Table 12 shows that the values of adsorption energy are listed in the following order: ZB3 (-1569.44kcal.mol^{-1}) > ZB4 (-1579.06 kcal.mol^{-1}), which corresponds to the classification of inhibition efficacy of quinazolinone-derived molecules acquired through experimental investigation. These values also demonstrate that the adsorption process is spontaneous.

4. CONCLUSION

The 2-(2-chlorophenyl)-2,3-dihydroquinazolin-4(1H)-one) and 2-(2,4-dichlorophenyl)-2, 3-dihydroquinazolin-4(1H)-one), named ZB3 and ZB4 showed good corrosion protection

properties for M steel in 1 M HCl solution, and the maximum protection efficiency is around 86% at an inhibitor concentration of 10^{-3} M. The PDP technique indicates that the inhibitors tested act as a mixed type. EIS measurements show that R_{ct} values increase with concentration, reaching maximum values of 237 Ω cm^2 and 240.2 Ω cm^2 for ZB3 and ZB4, respectively. On the other hand, n_{dl} values are higher than the free solution value and increase with concentration, indicating the adsorption of these 2 inhibitors onto the material surface.

Adsorption of ZB3 and ZB4 corresponds to the Langmuir isotherm, while thermodynamic results suggest that the adsorption mechanism is chemisorption. The results of DFT calculations and MC simulation showed reasonable correlations between the anticorrosion activity of the inhibitors tested and the properties of their chemical structure.

Declarations of interest

The authors declare no conflict of interest in this reported work.

REFERENCES

[1] M. Galai, M. Rbaa, M. Ouakki, K. Dahmani, S. Kaya, N. Arrousse, N. Dkhireche, S. Briche, B. Lakhrissi, and M. Ebn Touhami, Chem. Phys. Lett. 776 (2021) 138700.

[2] M. Hrimlaa, L. Bahsis, A. Boutouil, M. R. Laamari, M. Julve, and S. Stiriba, J. Mol. Structure 1231 (2021) 129895.

[3] B.A. Al Jahdaly, Y.R. Maghraby, A.H. Ibrahim, K.R. Shouier, A.M. Alturki, and R.M. El-Shabasy, Mater. Today Sustainability 20 (2022) 100242.

[4] M. Rbaaa, F. Benhiba, M. Galai, A.S. Abousalem, M. Ouakki, C.H. Lai, B. Lakhrissi, C. Jama, I. Waradi, M. EbnTouhamic, and A. Zarrouk, Chem. Phys. Lett. 754 (2020) 137771

[5] M. D. Pritzl, H. Tabatabai, and A. Ghorbanpoor, Int. J. Concr. Struct. Mater. 8 (2014) 201.

[6] M. Ouakki, M. Galai, M. Rbaa, A. S. Abousalem, B. Lakhrissi, M. EbnTouhami, and M. Cherkaoui, J. Mol. Liq. 319 (2020) 114063.

[7] F. Benhiba, H. Serrar, R. Hsissou, A. Guenbour, A. Bellaouchou, M. Tabyaoui, S. Boukhris, H. Oudda, I. Warad, and A. Zarrouk, Chem. Phys. Lett. 743 (2020) 137181.

[8] M. Galai, M. Rbaa, H. Serrar, M. Ouakki, A. Ech-chebab, A. S. Abousalem, E. Ech-chihbi, K. Dahmani, S. Boukhris, A. Zarrouk, and M. EbnTouhami, Physicochem. Eng. Aspects 613 (2021) 126127.

[9] M. Rbaa, M. Galai, M. ElFaydy, Y. ElKacimi, M. EbnTouhami, A. Zarrouk, and B. Lakhrissi, J. Mater. Environmental. Sci. 8 (2017) 3529.

[10] A. Tazouti, N. Errahmany, M. Rbaa, M. Galai, Z. Rouifi, R. Touir, A. Zarrouk, S. Kaya, M. EbnTouhami, B. El Ibrahimi, and S. Erkan, J. Mol. Structure 1244 (2021) 130976.

[11] N. Errahmany, M. Rbaa, A.S. Abousalem, A. Tazouti, M. Galai, H. ElKafssaoui, M. EbnTouhami, B. Lakhrissi, and R. Touir, J. Mol. Liq. 312 (2020) 113413.
[12] Z. Benzekri, H. Serrar, S. Boukhris, and A. Souizi, J. Turkish Chem. Soc. Section A: Chem. 4 (2017) 775.
[13] F. El hajri, Z. Benzekri, H. Anahmadi, S. Sibous, A. Ouasri, A. Souizi, A. Hassikou, and S. Boukhris, Inorganica Chim. Acta 536 (2022) 120915.
[14] M. Galai, M. El Gouri, O. Dagdag, Y. El Kacimi, A. Elharfi, and M. EbnTouhami, J. Mater. Environ. Sci. 7 (2016) 1562.
[15] A.D. Becke, Phys. Rev. A 38 (1988) 3098.
[16] M. Damej, R. Hsissou, A. Berisha, K. Azgaou, M. Sadiku, M. Benmessaoud, and N. Labjar, J. Mol. Structure 1254 (2022) 132425.
[17] M.W. Lee, D.Y. Jo, G.H. Han, and K.Y. Lee, Catalysis Today 397 (2022) 232.
[18] N.S. Abdelshafi, M.A. Sadik, M. A. Shoeib, and S.A. Halim, Arabian J. Chem. 15 (2022) 103459.
[19] H. A. Sarkhadi, and E. Asghri, Electrochim. Acta 54 (2008) 162.
[20] E. Naseri, M. Hajisafari, A. Kosari, M. Talari, S. Hosseinpour, and A. Davoodi, J. Mol. Liq. 269 (2018) 193.
[21] X. Li, S. Deng, and X. Xie, J. Corr. Sci. 81 (2014) 162.
[22] M. Rbaa, F. Benhiba, P. Dohare, L. Lakhrissi, R. Touir, B. Lakhrissi, A. Zarrouk, and Y. Lakhrissi, J. Chem. Data Collections 27 (2020) 100394.
[23] R. Agrawal, and T.K.G. Namboodhiri, J. Corr. Sci. 30 (1990) 37.
[24] B. Kumar, H. Vashisht, M. Goyal, A. Kumar, F. Benhiba, A.K. Prasad, S. Kumar, I. Baha dur, and A. Zarrouk, J. Mol. Liq. 318 (2020) 113890.
[25] N. Labjar, M. Lebrini, F. Bentiss, N.E. Chihib, S. El Hajjaji, and C. Jama, J. Mater. Chem. Phys. 119 (2010) 330.
[26] R.S. Gonçalves, D.S. Azambuja, and A.M.S. Lucho, J. Corrosion. Science 44 (2020) 467.
[27] D.K. Yadav, M.A. Quraishi, and B. Maiti, J. Corr. Sci. 55 (2012) 254.
[28] M. Behpour, S.M. Ghoreishi, N. Soltani, M. Salavati-Niasari, M. Hamadanian, and A. Gandomi, J. Corr. Sci. 50 (2008) 2172.
[29] H. A. Sorkhabi, D. Seifzadeh, and M.G. Hosseini, J. Corr. Sci. 50 (2008) 3363.
[30] Z. Tao, S. Zhang, W. Li, and B. Hou, J. Corr. Sci. 51 (2009) 2588.
[31] Y. Liu, X. Guo, D. Liu, Y. Wang, L. Hao, Y. Jin, and Y. C. Wu, J. Mol. Liq. 345 (2022) 117833.
[32] K. Sharma, A. Mudhoo, G. Jain, and J. Sharma, J. Green. Chem. Lett. Rev. 3 (2010) 7.
[33] M. Ouakki, M. Rbaa, M. Galai, B. Lakhrissi, E.H. Rifi, and M. Cherkaoui, J.Bio. Tribo. Corr. 4 (2018) 35.
[34] K.F. Khaled, J. Electrochim. Acta 53 (2008) 3484.
[35] S. Nesic, A. Kahyarian, and Y.S. Choi, Corr. 75 (2019) 274.

[36] K. Dahmani, M. Galai, M. Cherkaoui, A. El hasnaoui, and A. El Hessni, J. Mater. Environ. Sci. 8 (2017) 1676.

[37] R. Khrifou, R. Touir, A. Koulou, H. ElBakri, M. Rbaa, M. EbnTouhasmi, A. Zarrouk, and F. BenHiba, J. Surf. Interfaces. 24 (2021) 101088.

[38] H. Tayebi, H. Bourazmi, B. Himmi, A. ElAssyry, Y. Ramli, A. Zarrouk, A. Geunbour, and B. Hammouti, J. Der. Pharm. Chem. 6 (2014) 220.

[39] M. ElFaydy, R. Touir, M.E. Touhami, A. Zarrouk, C. Jama, B. Lakhrissi, L.O. Olasunkan mi, E. E. Ebenso, and F. Bentiss, J. Phys. Chem. Chem. Phys. 20 (2018) 20167

[40] O. Fergachi, F. Benhiba, M. Rbaa, M. Ouakki, M. Galai, R. Touir, B. Lakhrissi, H. Oudda, and M. EbnTouhami, J Bio. Tribo. Corr. 5 (2019) 21.

[41] A. Singh, K. R. Ansari, D. S. Chauhan, M. A. Quraishi, and S. Kaya, J. Sustainable. Chemistry. And. Pharmacy 16 (2020) 100257.

[42] M. Ramezanzadeh, G. Bahlakeh, and B. Ramezanzadeh, Journal. of. Molecular. Liquids 304 (2020) 112750.

[43] M. Kanwal, R. A. Khushnood, M. Shahid, and A. G. Wattoo, J. Cleaner. Production 355 (2022) 131785.

[44] A. Saady, Z. Rais, F. Benhiba, R. Salim, K. I. Alaoui, N. Arrousse, F. Elhajjaji, M. Taleb, K. Jarmoni, Y. K. Rodi, I. Warad, and A. Zarrouk, J. Corros. Sci. 189 (2021) 109621.

[45] S. Kumar, V. Kalia, M. Goyal, G. Jhaa, S. Kumar, H. Vashisht, H. Dahiya, M. A. Quraishi, and C. Verma, J. Mol. Liq. 357 (2022) 119077.

[46] M. Abouchane, N. Dkhireche, M. Rbaa, F. Benhiba, M. Ouakki, M. Galai, B. Lakhrissi, A. Zarrouk, and M. EbnTouhami, J. Mol. Liq. 360 (2022) 119470.

[47] G. Laadam, M. El Faydy, F. Benhiba, A. Titi, H. Amegroud, A. S. Al-Gorair, H. Hawsawi, R. Touzani, I. Warad, A. Bellaouchou, A. Guenbour, M. Abdallah, and A. Zarrouk, J. Mol. Liq. 375 (2023) 121268.

[48] G. Masuku, W. Nxumalo, M. M. Kabanda, L. C. Murulana, and I. Bahadur, J. Mol. Liq. 386 (2023) 122458.

[49] E. H. El Assiri, M. Driouch, J. Lazrak, Z. Bensouda, A. Elhaloui, M. Sfaira, T. Saffaj, and M. Taleb, Heliyon. 6 (2020) e05067.

[50] L. Zhang, A. Grimaud, R. Schwiedernoch, W. Y. Hernández, V. Ordomsky, and N. Naghavi, J. Electroanal. Chem. 903 (2021) 115820.

[51] K.F. Khaled, and M.M. Al-Qahtani, J. Mater. Chem. Phys. 113 (2009) 150.

[52] H. Lu, X. Ji, X. Ci, H. Zhu, Q. Wang, Y. Zong, and H. Tian, J. Eng. Asp. 674 (2023) 131892.

[53] K. Cherrak, F. Benhiba, N. K. Sebbar, E. M. Essassi, M. Taleb, A. Zarrouk, and A. Dafali, J. Chem. Data Collect. 22 (2019) 100252.

[54] A. Attou, M. Tourabi, A. Benikdes, O. Benali, H. B. Ouici, F. Benhiba, A. Zarrouk, C. Jama, and F. Bentiss, J. Eng. Asp. 604 (2020) 125320.

[55] S. Bousba, H. Allal, M. Damous, and S. Maza, J. Chem. 1225 (2023) 114168.
[56] B. Hni, N. K. Sebbar, E. H. Anouar, B. El Ibrahimi, M. Ellouz, T. Hökelek, J. T. Mague, M. Urrutigoîty, N. H. Ahabchane, and E. M. Essassi, J. Mol. Struct. 1221 (2020) 128886.